Microsatellite markers. Two hundred and fifty-six markers (Fig. 1) were used for the linkage analysis between C3H/HeN and CBA/JN mice. Amplification and labeling of specific microsatellite loci were performed by using the polymerase chain reaction (PCR) with FAM labeled primers. Amplified DNA was analyzed with automated fragment analyzer ABI3700 and genotyped by Genescan software (Applied Biosystems, Japan).

Linkage analysis. Genotype distribution was compared among affected and non-affected N1 mice. Since the trait distribution was similar, we performed non-

Chromosome 1 (53)									
	D1Mcg101	D1Mcg2	D1Mcg3	D1Mcg4	D1Mcg6	D1Mit120	D1Mit121	D1Mit160	D1Mit160
	D1Mit161	D1Mit167	D1Mit17	D1Mit171	D1Mit180	D1Mit19	D1Mit200	D1Mit211	D1Mit230
	D1Mit24	D1Mit242	D1Mit245	D1Mit251	D1Mit296	D1Mit3	D1Mit303	D1Mit316	D1Mit318
	D1Mit321	D1Mit322	D1Mit363	D1Mit372	D1Mit373	D1Mit374	D1Mit380	D1Mit410	D1Mit427
	D1Mit429	D1Mit430	D1Mit431	D1Mit432	D1Mit465	D1Mit518	D1Mit52	D1Mit52.2	D1Mit520
	D1Mit58	D1Mit64	D1Mit66	D1Mit67	D1Mit7	D1Mit70	D1Mit73	D1Mit75	
Chromosome 2 (25)									
	D2Mit106	D2Mit110	D2Mit139	D2Mit166	D2Mit169	D2Mit194	D2Mit200	D2Mit206	D2Mit226
	D2Mit255	D2Mit258	D2Mit265	D2Mit304	D2Mit305	D2Mit307	D2Mit311	D2Mit413	D2Mit443
	D2Mit456	D2Mit457	D2Mit496	D2Mit51	D2Mit6	D2Mit91	D2Mit92		
Chromosome 3 (11)									
	D3Mit200	D3Mit203	D3Mit230	D3Mit28	D3Mit29	D3Mit3	D3Mit305	D3Mit323	D3Mit361
	D3Mit46	D3Mit90							
Chromosome 4 (37)									
	D4Mit116	D4Mit122	D4Mit126	D4Mit134	D4Mit146	D4Mit169	D4Mit18	D4Mit180	D4Mit181
	D4Mit190	D4Mit203	D4Mit219	D4Mit225	D4Mit226	D4Mit227	D4Mit234.2	D4Mit251	D4Mit255
	D4Mit26	D4Mit27	D4Mit272	D4Mit285	D4Mit310	D4Mit33	D4Mit331	D4Mit336	D4Mit348
	D4Mit354	D4Mit357	D4Mit42	D4Mit43	D4Mit45	D4Mit65	D4Mit71	D4Mit81	D4Mit84
	D4Nds3								
Chromosome 5 (22)									
	D5Mit10	D5Mit101	D5Mit108	D5Mit115	D5Mit13	D5Mit134	D5Mit23	D5Mit233	D5Mit239
	D5Mit254	D5Mit26	D5Mit291	D5Mit297	D5Mit314	D5Mit338	D5Mit348	D5Mit371	D5Mit406
	D5Mit425	D5Mit65	D5Mit79	D5Mit93					
Chromosome 6 (4)									
	D6Mit345	D6Mit366	D6Mit8	D6Mit254					
Chromosome 7 (5)									
	D7Mit232	D7Mit259	D7Mit27	D7Mit39	D7Nds5				
Chromosome 8 (3)									
	D8Mit14	D8Mit224	Mt2(D8Mit15)						
Chromosome 9 (3)									
	Cyp1a2(ch#9)		D9Mit2	D9Mit279					
Chromosome 10 (16)									
	D10Mit115	D10Mit134	D10Mit15	D10Mit150	D10Mit186	D10Mit20	D10Mit209	D10Mit214	D10Mit230
	D10Mit261	D10Mit266	D10Mit282	D10Mit297	D10Mit313	D10Mit36	D10Mit61		
Chromosome 11 (3)									
	D11Mit157	D11Mit2	Hoxb(Ch#11)						
Chromosome 12 (4)									
	D12Mit158	D12Mit190	D12Mit231	D12Mit292					
Chromosome 13 (9)									
	D13Mit110	D13Mit186	D13Mit24	D13Mit253	D13Mit26	D13Mit283	D13Mit35	D13Mit48	D13Mit69
Chromosome 14(3)									
	D14Mit2	D14Mit95	D14Nds5						
Chromosome 15(5)									
	D15Mit234	D15Mit29	D15Mit34	D15Mit6	D15Mit90				
Chromosome 16 (7)									
	D16Mit110	D16Mit13	D16Mit211	D16Mit5	D16Mit57	D16Mit88	D16Mit94		
Chromosome 17 (11)									
	D17Mit11	D17Mit119	D17Mit152	D17Mit155	D17Mit176	D17Mit21	D17Mit221	D17Mit266	D17Mit51
	D17Mit52	D17Mit96							
Chromosome 18 (3)									
	D18Mit3	D18Mit40	D18Mit60						
Chromosome 19 (7)									
	D19Mit10	D19Mit10	D19Mit128	D19Mit18	D19Mit8	D19Mit85	D19Mit90		
Chromosome X (25)									
	DXMit119	DXMit121	DXMit143	DXMit149	DXMit154	DXMit156	DXMit16	DXMit189	DXMit197
	DXMit199	DXMit236	DXMit248	DXMit249	DXMit31	DXMit5	DXMit54	DXMit55	DXMit64
	DXMit67	DXMit73	DXMit74	DXMit84	DXMit89	DXMit95	DXMit99		

Fig. 1. A list of markers examined difference between C3H and CBA mouse in a total 256 markers.

parametric statistical analysis for establishing genetic linkage. Contingency tables consisting of affected and non-affected C3H/C3H and C3H/CBA strains were constructed, and chi square (χ^2) tests were performed with one degree of freedom. As recommended by Lander and Kruglyak, $P<0.0034$ ($\chi^2>8.58$) were the thresholds for suggestive linkage (10).

Production of inflammatory cytokines after exposure to CADS. To clarify the inflammatory cytokine response against CADS, we also examined the sequential change of serum cytokines after intraperitoneal injection of CADS. Twenty milligrams of CADS suspended in 0.2 ml of PBS(−) was injected intraperitoneally to C3H/HeN. Sera were obtained from sacrificed mice at each time ($N=5$) for 14 days after injection of CADS and then frozen at −80 C. Serum cytokines, such as interleukins IL-1β, IL-4, IL-6, IL-12, TNF-α, and IFN-γ were measured by using ELISA assay kits: IL-1β, IL-4, IL-6, IL-12, and TNF-α (Genzyme, Mass., U.S.A.), and IFN-γ (Pierce ENDOGEN, Qld, Australia).

Results

Histological Observations of Arteritis

Table 1 shows the incidence of vasculitis in the coronary artery and/or the aortic root in (CBA/JN×C3H/HeN)F1, (C3H/HeN×CBA/JN)F1, and [(CBA/JN×C3H/HeN)×C3H/HeN]N1 was 0%, 16.7%, and 20.7% respectively, while that in C3H/HeN parents was 71.1% (27/38), but in CBA/JN absence (0%, 0/27). Most cases of vasculitis were observed in the aortic root and/or the coronary artery (Fig. 2). All layers of these vessels showed severe inflammation, which is defined as 'productive granulomatous inflammation, but fibrinoid necrosis was rarely determined.' Intima showed various degrees of fibrocellular thickening associated with the lumen of coronary artery became stenotic. In addition to the disruption of internal and external elastic laminas, smooth muscle cells in media deteriorated from severe inflammation. Furthermore, the destruction of the normal structure of the coronary artery in some cases caused aneurismal dilatation. However, neither thrombotic occlusion nor myocardial infarction was observed. Histological differences of arteritis between N1 and C3H/HeN was not elucidated. Arteritis in other visceral organs such as renal artery, testicular artery, and abdominal aorta were rarely detected.

Linkage Analysis with Chromosome Mapping

Two hundred and fifty-six microsatellite markers were tested to segregate loci by original parental strains (Fig. 1). However, most markers were the same sequence length polymorphism between C3H/NeN and CBA/JN. Only 48 markers were selected for the linkage analysis (Table 2). Genome-wide interval mapping analysis between coronary artery and genetic markers for the identification of susceptibility loci was performed by using χ^2 test as described in "Materials and Methods." The markers on the chromosome 1 showed the association even though possibility on other chromosome loci may exist. Two of 11 markers on chromosome 1, *D1Mit171* and *D1Mit245* around 20.2 cM revealed suggestive linkage with P value of 0.0019 (Table 3). The other markers on chromosome 1 did not indicate the association. Based on the suggestive level of *D1Mit171* and *D1Mit245*, this region is thought to influence to the development of coronary arteritis. On the other chromosomes, the marker, *D4Mit285*, showed low probability of 0.017, but was not in the scope to designate an association.

Table 1. Affected rate of coronary arteritis after 9 weeks challenge with CADS

Mice	Affected rate (%)
C3H/HeN	71.1 (27/38)
CBA/JN	0 (0/27)
(C3H male×CBA female) F1	0 (0/9)
(C3H female×CBA male) F1	16.7 (1/6)
(CBA female×C3H male) F1×C3H	20.7 (24/115)

CBA/JN and C3H/HeN (CBA/JN×C3H/HeN) and N1 backcross progeny between F1 and C3H/HeN [(CBA/JN×C3H/HeN)×C3H/HeN] were prepared.

Circulation of Inflammatory Cytokines after Exposure to CADS

Sequential changes of inflammatory cytokines IL-12, IL-1β, TNF-α, IL-6, IFN-γ, and IL-4 in serum for 14 days after intraperitoneal injection of CADS were measured by ELISA assay. Both IL-1β and IL-12 levels in serum increased at 1 hr after injection of CADS, and then decreased gradually, but IL-12 did not decrease like profile of IL-1β (Fig. 3a). After increases of IL-1β and IL-12, levels of TNF-α and IL-6 peaked at 3 hr after the injection, and then restored to baseline by 24 hr (Fig. 3b). Levels of IFN-γ gradually increased over the same period, but no change in IL-4 level was noted (Fig. 3c).

Discussion

Some infectious microorganisms have been implicated in the etiology of KD, though primary causes remain an enigma (6, 11, 16, 22). These candidates of etiology may act as initial trigger to induce arteritis. The spontaneous arteritis model may not be well suited for study-

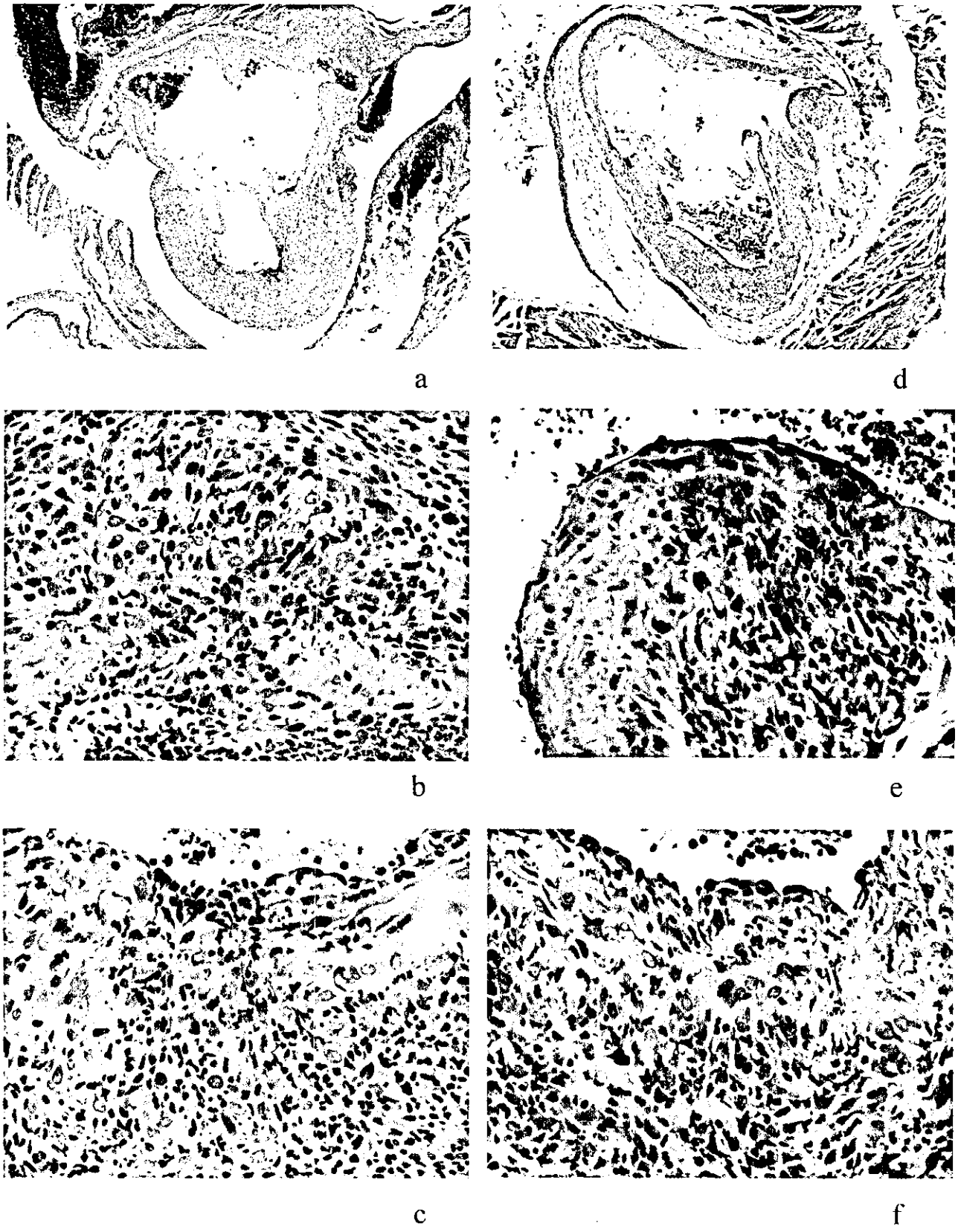

Fig. 2. Histological feature of coronary arteritis in N1 and C3H/HeN. (a) Vasculitis at the coronary artery and aortic root in N1 mouse (HE stain, ×40), (b) coronary arteritis in N1 mouse (HE stain, ×400), (c) aortitis in N1 mouse (HE stain, ×400), (d) coronary arteritis and aortitis in C3H/HeN (HE stain, ×40), (e) coronary arteritis in C3H/HeN (HE stain, ×400), (f) aortitis in C3H/HeN (HE stain, ×400).

Table 2. A list of the 48 markers used for the linkage analysis from 256 candidates for markers

Chromosome	Symbol	Position (cM)	Chromosome	Symbol	Position (cM)
1	D1Mit374	19.0	6	D6Mit345	46.0
1	D1Mit171	20.2	7	D7Mit232	26.8
1	D1Mit245	20.2	8	D8Mit224	17.0
1	D1Mit75	32.1	8	Mt2	45.0
1	D1Mit380	36.9	8	D8Mit14	67.0
1	D1Mit251	38.1	9	D9Mit2	17.0
1	D1Mcg3	38.9	9	Cyp1a2	31.0
1	D1Mcg6	39.9	9	D9Mit279	67.0
1	D1Mit7	41.0	10	D10Mit214	19.0
1	D1Mit200	80.0	11	Hoxb	56.0
1	Tgfbm2	106.3	12	D12Mit231	48.0
2	D2Mit92	41.4	13	D13Mit110	47.0
2	D2Mit206	51.4	14	D14Mit2	5.0
2	D2Mit311	83.1	14	Nfl	28.7
2	D2Mit456	86.3	15	D15Mit6	13.7
2	D2Mit265	105.0	16	D16Mit5	38.0
2	D2Mit200	107.0	17	D17Mit96	54.6
2	D2Mit457	108.0	18	D18Mit60	16.0
3	D3Mit90	4.6	19	D19Mit128	10.9
3	D3Mit200	77.3	19	D19Mit10	47.0
3	D3Mit323	84.9	X	DXMit74	20.0
4	D4Mit272	21.9	X	DXMit16	37.0
4	D4Mit285	71.0	X	DXMit121	67.0
4	D4Mit357	81.5			
5	D5Mit101	81.0			

Table 3. A list of markers that exhibited distribution disequilibrium from the 2×2 χ^2 based on a ratio of affected C3H/C3H:C3H/CBA to non-affected

Chromosome	Distance (cM)	Marker	Affected / Non-affected	χ^2	Probability
1	19.0	D1Mit374	18:6 / 34:45	7.52	0.0061
	20.2	D1Mit171	19:5 / 34:45	9.62	0.0019[a]
	20.2	D1Mit245	19:5 / 34:45	9.62	0.0019[a]
	32.1	D1Mit75	18:6 / 33:46	8.13	0.0044
	38.1	D1Mit251	17:7 / 30:49	8.01	0.0046
	38.9	D1Mcg3	15:9 / 31:48	4.03	0.0447
	39.9	D1Mcg6	15:9 / 31:48	4.03	0.0447
	41.0	D1Mit7	15:9 / 31:48	4.03	0.0447
4	71.0	D4Mit285	7:17 / 45:34	5.69	0.0171

[a] Suggestive linkage.

ing KD, because it requires an initial trigger from some infectious microorganisms to induce arteritis. On the other hand, our model requires injection of CADS to induce arteritis. This model is very useful for the study of the pathogenesis of arteritis in KD for two main reasons: 1) both the histological features and distribution of arteritis are similar to that of KD, and 2) infectious agents are required to induce the development of arteritis. The mechanisms of developing arteritis in patients with KD are still unclear; however, several reports have

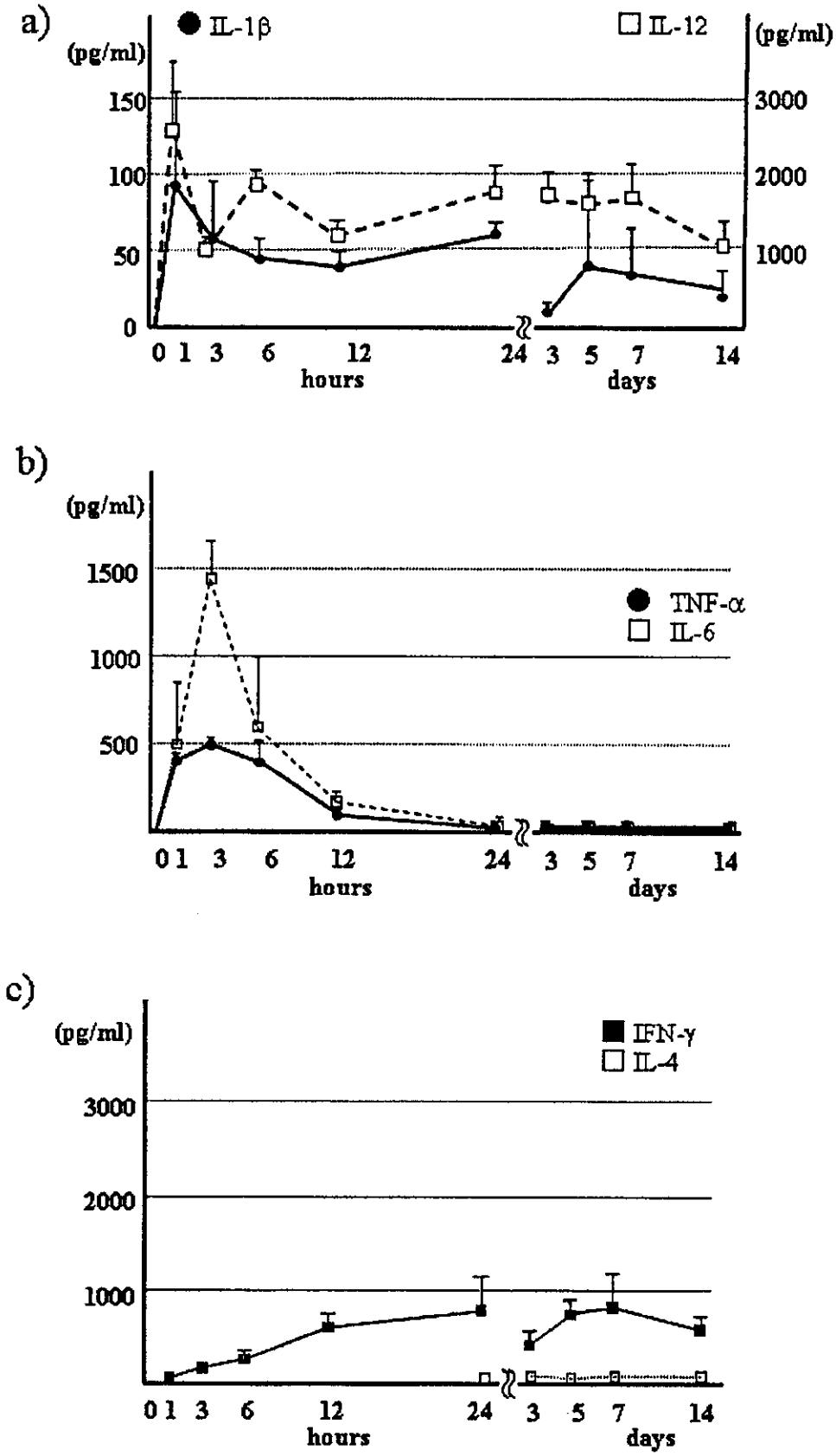

Fig. 3. Time course of serum cytokines after intraperitoneal injection of CADS. (a) Time course of serum IL-1β and IL-12 after injection of CADS, (b) time course of serum TNF-α and IL-6 after injection of CADS, (c) time course of serum IFN-γ and IL-4 after injection of CADS.

discussed the role of inflammatory cytokines in patients with a genetic predisposition to developing coronary arteritis (7, 8). The animal model is considered to be very useful for clarifying the pathogenesis of arteritis in these patients and may allow for the identification of specific treatments for the disease. With the observed differences in the incidence of arteritis in C3H/HeN mice and CBA/JN mice, it can be derived that genetic differences of the mouse strains does influence arteritis. Therefore, it was considered that C3H/HeN may express or attenuate the expression of genes that govern the susceptibility to coronary arteritis.

In the present study, we showed that the loci governing suggestive susceptibility to coronary arteritis were situated on chromosome 1 even though possibility on other chromosome loci may exist. Two of 11 markers on chromosome 1, *D1Mit171* and *D1Mit245* (map position 20.2 cM), appeared to be involved in the susceptibility loci to the development of coronary arteritis. This chromosomal region influences the IL-1 receptors types 1 and 2 (*Il1r1* and *Il1r2*, 19.5 cM). In addition, our results here revealed that IL-1β in sera rapidly increased after intraperitoneal injection of CADS. These findings suggest a ligand-receptor interaction between IL-1β and the IL-1 receptor, which may affect the onset of arteritis. It has been reported that IL-1β regulates vascular damage *in vitro*. Specifically, IL-1β directly injures endothelial cells; however, mechanisms of endothelial cell injury are unclear. Interestingly, an indirect role of IL-1β in the regulation of neutrophil-mediated killing of endothelial cells has been reported (3, 4, 12, 18). Adhesive interaction between activated neutrophils and endothelial cells was facilitated by exposure to IL-1β and superoxide anion, produced by activated neutrophils, and subsequently damaged neighboring endothelial cells (1).

One of the peculiar histological features of arteritis in this model was the severe neutrophilic infiltration observed in the afflicted artery, suggesting an important role of neutrophil activation in the development of arteritis. In addition, it has been reported that the specific antigen to autoantibodies, myeloperoxidase-anti-neutrophil cytoplasmic antibody (MPO-ANCA), targeting its antigen MPO were closely related to the development of coronary arteritis using MPO-deficient mice (17). It is considered that coronary arteritis in this model must be genetically regulated by interactions between neutrophils and endothelial cells modulated by IL-1β. Furthermore, the allelic polymorphism of both *Il1r1* and *Il1r2* and the functional relevance of their polymorphism may be a necessity.

On the other hand, *D4Mit285* (map position 71.0 cM) on chromosome 4 showed negative effect against affectability to coronary arteritis, however this marker showed a probability of 0.017. Several genes related to inflammation are coded around *D4Mit285* on chromosome 4, including TNF receptor superfamily member 1b, 8, and 9 (*Tnfrsf1b*, *Tnfrsf8*, and *Tnfrsf9*) (75.5 cM). The functional relevance of this is seen with the rapid increase of TNF-α following elevation of IL-1β after exposure to CADS. There are also studies that claim IL-1β and TNF-α can induce endothelial cell injury by activated neutrophils (3, 4, 12, 18). Therefore, some of these genes are considered to be protective against the development of coronary arteritis, even in the susceptible C3H/HeN strain. However, the marker *D2Mit265* (χ^2=3.61, P=0.058) on chromosome 2, on which IL-1β is located, did not indicate a significant difference. Th-1 cytokines, such as IL-12 and IFN-γ were also produced by exposure of CADS. It was considered that Th-1 type immunity might have an influence on the development of arteritis in this model; however, we have no direct evidence in the present study to determine whether or not the genes of these cytokines affected the coronary arteritis outcome, since the number of microsatellite markers was insufficient to examine these genomic regions.

The difference in the incidence of coronary arteritis between C3H/HeN and CBA/JN may be attributed to differences in the regulation of genes encoding inflammatory cytokines. It may be concluded from the present study that the development of coronary arteritis is multi-factorial and controlled with cumulative effects of these multiple gene loci in this mouse model.

The authors thank Ms. Hitomi Yamada for her technical assistance and, Drs. Kei Takahashi in Toho University Medical School, Akiko Okawara in National Institute of Infectious Diseases and Masato Nose in Ehime University Medical for their helpful discussion in this work. This study was supported in part by Project Research Grants No. 11-26, 12-30, and 13-19 from the Toho University School of Medicine, Ministry of Education, Culture, Sports, Science and Technology for KT and KS, Ministry of Health, Labour and Welfare for KT and KS, Japan Health Science Foundation for KS, and a research fellowship from the Japan Society for the Promotion of Science for ASP. All experiments described in this study were performed in accordance with the current laws of Toho University and National Institute of Infectious Diseases in Japan.

References

1) Alex, B.L., and Peter, A.W. 2000. Regulation of inflammatory vascular damage. J. Pathol. **190**: 343–348.
2) Atobe, T., and Murata, H. 1987. Morphological studies of experimental arteritis—relation with coronary arteritis in Kawasaki disease—. Angiology **27**: 625–633.
3) Borgmann, S., Endisch, G., Hacker, U.T., Song, B.S., and

Fricke, H. 2003. Proinflammatory genotype of interleukin-1 receptor antagonist is associated with ESRD in proteinase 3-ANCA vasculitis patients. Am. J. Kidney Dis. **41**: 933–942.
4) Gonzalez-Gay, M.A., Di Giovine, F.S., Silvestri, T., Amoli, M.M., Garcia-Porrua, C., Thomson, W., Ollier, W.E., and Hajeer, A.H. 2002. Lack of association between IL-1 cluster and TNF-alpha gene polymorphism and giant cell arteritis. Clin. Exp. Rheumatol. **20**: 431.
5) Gu, L., Weinreb, A., Wang, X.P., Zack, D.J., Qiao, J.H., Weisbart, R., and Lusis, A.J. 1998. Genetic determinants of autoimmune disease and coronary vasculitis in the MRL-lpr/lpr mouse model of systemic lupus erythematosus. J. Immunol. **161**: 6999–7006.
6) Hamashima, Y., Tasaka, K., Hoshino, T., Nagata, N., Furukawa, F., Kao, T., and Tanaka, H. 1982. Mite-associated particles in Kawasaki disease. Lancet **2**: 266.
7) Jibiki, T., Terai, M., Shima, M., Ogawa, A., Hamada, H., Kanazawa, M., Yamamoto, S., Oana, S., and Kohno, Y. 2001. Monocyte chemoattractant protein 1 gene regulatory region polymorphism and serum levels of monocyte chemoattractant protein 1 in Japanese patients with Kawasaki disease. Arthritis Rheum. **44**: 2211–2212.
8) Kamizono, S., Yamada, A., Higuchi, T., Kato, H., and Itoh, K. 1999. Analysis of tumor necrosis factor-alpha production and polymorphisms of the tumor necrosis factor-alpha gene in individuals with a history of Kawasaki disease. Pediatr. Int. **41**: 341–345.
9) Kawasaki, T., Kosaki, F., and Okawa, S. 1974. A new infantile acute febrile mucocutaneous syndrome (MCLS) prevailing in Japan. Pediatrics **54**: 271–276.
10) Lander, E., and Kruglyak, L. 1995. Genetic dissection of complex traits: guidelines for interpreting and reporting linkage results. Nat. Genet. **11**: 241–247.
11) Meissner, H.C., and Leung, D.Y. 2000. Superantigens, conventional antigens and the etiology of Kawasaki syndrome. Pediatr. Infect. Dis. **19**: 91–94.
12) Meyrick, B., Christman, B., and Jesmok, G. 1991. Effects of recombinant tumor necrosis factor-alpha on cultured pulmonary artery and lung microvascular endothelial monolayers. Am. J. Pathol. **138**: 93–108.
13) Murata, H. 1979. Experimental *Candida*-induced arteritis in mice, relation to arteritis in the mucocutaneous lymph node syndrome. Microbiol. Immunol. **23**: 825–831.
14) Naoe, S., Atobe, T., and Murata, H. 1983. Experimental coronary arteritis induced by an alkali extract of *Candida albicans* in stool of Kawasaki disease patient. Pediatr. Jpn. **23**: 257–261.
15) Naoe, S., Takahashi, K., Masuda, H., and Tanaka, N. 1991. Kawasaki disease. With particular emphasis on arterial lesions. Acta Pathol. Jpn. **41**: 785–797.
16) Ohkuni, H., Todome, Y., Mizuse, M., Ohtani, N., Suzuki, H., Igarashi, H., Hashimoto, Y., Ezaki, T., Harada, K., and Imada, Y. 1993. Biologically active extracellular products of oral viridans streptococci and the aetiology of Kawasaki disease. J. Med. Microbiol. **39**: 352–362.
17) Okawara, I.A., Oharaseki, T., Takahashi, K., Hashimoto, Y., Aratani, Y., Koyama, H., Maeda, N., Naoe, S., and Suzuki, K. 2001. Contribution of myeloperoxidase to coronary artery vasculitis associated with MPO-ANCA production. Inflammation **25**: 381–387.
18) Schuger, L., Varani, J., Marks, R.M., Kunkel, S.L., Johnson, K.J., and Ward, P.A. 1989. Cytotoxicity of tumor necrosis factor-alpha for human umbilical vein endothelial cells. Lab. Invest. **61**: 62–68.
19) Takahashi, K., Oharaseki, T., and Naoe, S. 2001. Pathological study of postcoronary arteritis in adolescents and young adults: with reference to the relationship between sequelae of Kawasaki disease and atherosclerosis. Pediatr. Cardiol. **22**: 138–142.
20) Takahashi, K., Oharaseki, T., Wakayama, M., Yokouchi, Y., Naoe, S., and Murata, H. 2004. Histopathological features of murine systemic vasculitis caused by *Candida albicans* extract—an animal model of Kawasaki disease. Inflamm. Res. **53**: 72–77.
21) Yamada, A., Miyazaki, T., Lu, L.-M., Ono, M., Ito, R.M., Terada, M., Mori, S., Hata, K., Nozaki, Y., Nakatsuru, S., Nakamura, Y., Onji, M., and Nose, M. 2003. Genetic basis of tissue specificity of vasculitis in MRL/lpr mice. Arthritis Rheum. **48**: 1445–1451.
22) Yoshioka, T., Matsutani, T., Toyosaki, M.T., Suzuki, H., Uemura, S., Suzuki, R., Koike, M., and Hinuma, Y. 2003. Relation of streptococcal pyogenic exotoxin C as a causative superantigen for Kawasaki disease. Pediatr. Res. **53**: 403–410.

Microbiol. Immunol., 48(12), 985–994, 2004

Editor-Communicated Paper

Quantum Dots Targeted to the Assigned Organelle in Living Cells

Akiyoshi Hoshino[1,2,3], Kouki Fujioka[1], Taisuke Oku[1,4], Shun Nakamura[5], Masakazu Suga[1], Yukio Yamaguchi[4], Kazuo Suzuki[3], Masato Yasuhara[2], and Kenji Yamamoto*[,1,2]

[1]Department of Medical Ecology and Informatics, Research Institute, International Medical Center of Japan, Shinjuku-ku, Tokyo 162–8655, Japan, [2]Department of Pharmacokinetics and Pharmacodynamics, Hospital Pharmacy, Tokyo Medical and Dental University, Bunkyo-ku, Tokyo 113–8519, Japan, [3]Department of Bioactive Molecules, National Institute of Infectious Diseases, Shinjuku-ku, Tokyo 162–8640, Japan, [4]Department of Chemical System Engineering, School of Engineering, University of Tokyo, Bunkyo-ku, Tokyo 113–8656, Japan, and [5]Division of Biochemistry and Cellular Biology, National Institute of Neuroscience, Kodaira, Tokyo 187–8502, Japan

Communicated by Dr. Hidechika Okada: Received October 8, 2004. Accepted October 21, 2004

***Abstract*: Fluorescent nanocrystal quantum dots (QDs) have the potential to be applied to bioimaging since QDs emit higher and far longer fluorescence than conventional organic probes. Here we show that QDs conjugated with signal peptide obey the order to transport the assigned organelle in living cells. We designed the supermolecule of luminescent QDs conjugated with nuclear- and mitochondria-targeting ligands. When QDs with nuclear-localizing signal peptides were added to the culture media, we can visualize the movements of the QDs being delivered into the nuclear compartment of the cells with 15 min incubation. In addition, mitochondrial signal peptide can also transport QDs to the mitochondria in living cells. In conclusion, these techniques have the possibility that QDs can reveal the transduction of proteins and peptides into specific subcellular compartments as a powerful tool for studying intracellular analysis *in vitro* and even *in vivo*.**

***Key words*: Quantum dot, Signal peptide, Nanocrystal, Nuclear localizing signal, Mitochondria targeting signal, Bioimaging**

Nanotechnology is the technology of designing, manufacturing, and utilizing the "supermolecule materials" which have the specific function based on their nanometer size. The "supermolecule" said here is a functional unit of two meanings; (1) A supermolecule consists of each molecule that has a certain mutual interaction and relation with one another, (2) A supermolecule shows its specific function as a whole molecule. Ultrafine nanocrystals have been expected to be applied widely in biomedical fields as biomaterials, immunoassay, diagnostics, and even in therapeutics (7, 9, 18, 32, 34, 40, 41). One of them, nanocrystal quantum dots (QDs), is widely used as stable and bright fluorophores that can have high quantum yields, narrow luminescent spectra, high absorbency, high resistance to photobleaching, and can provide excitation of several different emission colors using a single wavelength for excitation (4, 19).

In the field of molecular biology, fluorescent tagging of cells and biomolecules with organic fluorophores such as FITC has been used for a long time for these purposes of tracking biomolecules. But unfortunately, the use of organic fluorophores for living-cell applications is subject to certain limitations, because most of fluorophores photobleach easily (17). These organic fluorophores have their broad emission bands, which limit the number of fluorescent probes that can be simultaneously resolved. In addition, there are a lot of bright fluorophores, such as Hoechst® dyes and a rhodamine 123 derivative (Mitotracker®) (20), used for stain of nuclei and mitochondria, but these fluorophores cannot transport proteins or other molecules to the target

**Address correspondence to* Dr. Kenji Yamamoto, Department of Medical Ecology and Informatics, Research Institute, International Medical Center of Japan, Toyama 1–21–1, Shinjuku-ku, Tokyo 162–8655, Japan. Fax: +81–3–3202–7364. E-mail: backen@ri.imcj.go.jp

Abbreviations: MPA, 3-mercaptopropanoic acid; QD, quantum dot; TOPO, *n*-trioctylphosphine oxide.

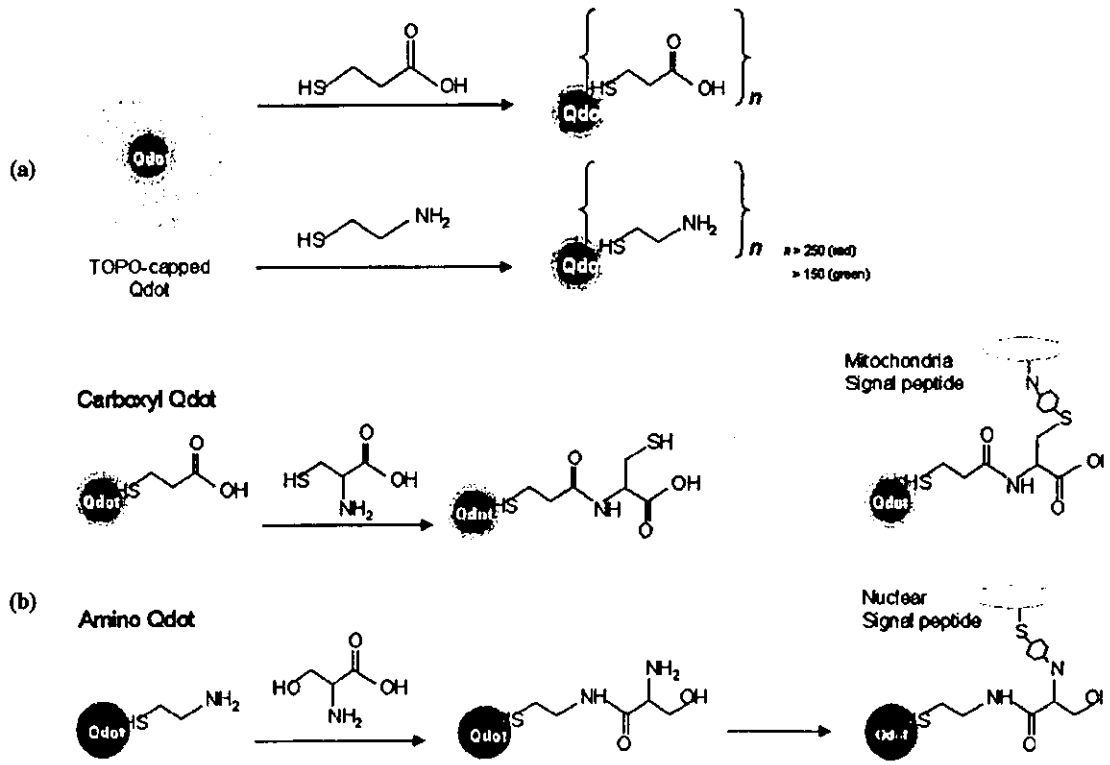

Fig. 1. Schematic illustration of peptide conjugated QDs for organelle targeting and imaging. (a) Chemically synthesized TOPO-capped QDs were replaced by MPA or cysteamine using thiol-exchange reactions. After reaction, QDs were covered with approximately 250 carboxyl or amine groups per particle. (b) A two-step conjugation strategy of QD-oligopeptide probes. MPA-QD (upper lane) or cysteamine-QD (lower lane) was primarily coupled with amine groups of cysteine or serine by using EDC coupling reagents. Then amino acid-coated QDs were secondarily conjugated with target peptides by coupling between *N*-hydroxysuccinimidyl and maleimide groups.

organelle. On the other hand, the signal peptides with organic fluorophore cannot trace the luminescent for long time observation. In contrast, QDs are stabilized over a far longer exposure-time to light and can emit fluorescence of higher luminosity than the conventional organic fluorescence probes (5, 8, 27). Therefore, QDs are suitable for designing the supermolecule that supplemented the biological effects to itself, and applications with QDs are now widely performed as long-time fluorescent markers for efficient collection of fluorescence (3, 17, 22, 24, 35).

Once our synthesized QDs were enfolded into the hydrophobic micelles and completely dissolved in aqueous solution, which promotes several innovations to improve the solubility to apply for biological methods (2, 10, 11, 23). The water-soluble QDs in our previous method have lower stability for low pH or salt-containing buffer (14). There is very little amount of conjugate by using these QDs, since the most of QDs were easily aggregated under the conditions that combine QD with peptides or protein. Therefore, we could only utilize QDs as the high fluorescence cell-tracking markers (14, 33). We previously reported that several novel surface-modified QDs using carboxylic acids, polyalcohols, or amines showed various physicochemical properties (16). In this article, we established a two-step conjugating method as shown in Fig. 1. The QDs of carboxyl groups were primarily coupled with amine groups of cysteine monomer, and QDs of amine groups were with carboxylic groups of serine monomer, respectively. The obtained amino acid-coated QDs, which were stable for the pH changes, were secondarily conjugated with target peptides/proteins by using their sulfhydryl and amine groups.

Some proteins and peptides have been demonstrated to penetrate through the plasma membrane of cells by their protein transduction domains (12, 21, 26, 31). Previous studies defined that protein transduction by nuclear localizing peptides was an efficient method to deliver proteins into the nuclei of cells (25, 37). In this study we tried to label two functional oligopeptides transported to nuclear localizing or mitochondria, and

evaluated whether QD-peptide complex worked as the specific functional supermolecule based on original peptides.

Materials and Methods

Synthesis of hydrophilic QDs. Synthesis of ZnS-coated CdSe nanocrystal QDs (fluorescence wavelength: approximately 642 nm emitted red, and approximately 518 nm emitted green), which were enfolded into the micelle of *n*-trioctylphosphine oxide (TOPO), was previously reported (6, 15). 3-Mercaptopropanoic acid (MPA) and 2-aminoethanethiol (cysteamine hydrochloride) were used to obtain two kinds of hydrophilic QDs (carboxyl- and amino-QDs) by thiol exchange methods. In the case of carboxyl-QD, 50 mg of TOPO-QDs were dissolved into 1 ml tetrahydrofuran (THF) in a 4 ml-volume flasket, and then 250 μl MPA (Sigma-Aldrich, St. Louis, Mo., U.S.A.) were added. Then the mixture was heated at 85 C for 24 hr. In the case of amino-QD, primarily 250 mg cysteamine (Wako Pure Chemicals, Tokyo) was heated at 85 C in a flask (16). After melting, 50 mg/ml TOPO-QDs in THF was dropped to the flask and heated at 85 C for 2 hr. After the reaction, the turbid solution was collected and centrifuged at maximum speed. After it dried up, purified water was added to the residue, and centrifuged at maximum speed to remove the insoluble residue. The supernatant fraction containing soluble QDs was collected. After purified by Sephadex G-25 column (Amersham Biosciences, Piscataway, N.J., U.S.A.), QDs were concentrated and powderized by vacuum distillation. QDs were reconstituted in purified water before use.

Preparation of peptide-conjugated QDs. Amino acid sequences of three well-known functional oligopeptides described below were chemically synthesized; nuclear localizing peptide ($R_{11}KC$, sequenced NH_2-RRRRRRRRRRRKC-COOH) (25), mitochondria targeting signal sequence of cytochrome-*c* oxidase VIII subunit (Mito-8, sequenced NH_2-MSVLTPLLLRGLTGSARRLPVPRAKIHWLC-COOH) (13) or control mitochondrial peptide (START, sequenced NH_2-STARTSTARTSTARTSC-COOH) (1). The peptides were conjugated to QDs by a two-step reaction. Initially, 100 μM QD solution was mixed with equal volume of 100 mM cysteine solution in coexistent with 100 mM EDC coupling reagents (Pierce Biotechnology, Rockford, Ill., U.S.A.) and continuously mixed at 4 C for 1 hr. After removed of free-amino acid by Nap-5 column (Amersham Biosciences), about 10-fold mol of target peptides were secondarily conjugated with QD by using sulfo-SMCC coupling reagents (Pierce Biotech) and sonicated for 2 hr at 4 C. Products were purified using ultra-filtration membrane (NMWL 10000, Centriprep® Millipore). Finally, purified QD-peptide conjugates were filtrated with 0.1-μm membrane filters (Millipore) before use. To analyze the protein content of QD-conjugated peptides, conjugated QDs was plated to 96-well microplate and RC-DC Protein Assay reagent (Bio-Rad, Hercules, Calif., U.S.A.) was added. Six hundred fifty nanometer absorbance was measured by microplate reader (Bio-Rad). MPA-coated QD without coupling with any peptides was used as negative control.

Assessment of QD-uptake by cells. Vero cells were cultured in DMEM/F12 supplemented with 5% heat-inactivated fetal bovine serum at 37 C. To avoid the non-specific binding of QDs on the glass, 10 mm glass-based culture dish (Matsunami Glass Industries, Japan) was pre-coated with poly-L-lysine (Peptide Institute Co., Ltd., Osaka, Japan). The cells were plated at a volume of 1×10^5 cells/well on a glass-based dish. Then cells were stimulated with the indicated concentration of QD-peptides. After incubation, the cells were washed with PBS 5 times to remove the non-specific binding QDs, and the cells were fixed, and embedded in the glycerol containing 0.1% sodium azide. In the case of co-localization assay, cells were observed with a confocal microscopy MRC-1024 (Bio-Rad). Time course of $R_{11}KC$-coated QDs was examined on the fluorescence microscopy system equipped with a CO_2 incubator (IM-310 cell-culture microscope system, Olympus, Japan). Images were acquired with a digital camera D1X (Nikon) under fluorescent microscopy IX-81 (Olympus) using WIR mirror unit to adjust excitation wavelength over 610 nm.

Results and Discussion

Some oligopeptides have been demonstrated to penetrate across the cellular membrane by their protein transduction domains and specifically located to their designated organelle (12, 21, 26, 31). Previous studies showed that the protein transduction by nuclear localizing signal oligopeptide was an efficient method of delivering proteins into the nuclei of cells (37). To establish the supermolecule design that supplemented the biological effects to nanocrystal, we conjugated two kinds of functional NLS and MTS oligopeptides, which were transported to nuclear or mitochondria (13, 25). Then we evaluated that QD-peptide complex worked as the specific supermolecule those functions were based on their original peptides.

For the achievements of assemble QD-supermolecule, we established a two-step conjugating method as shown in Fig. 1. Briefly, QDs were coupled with amino

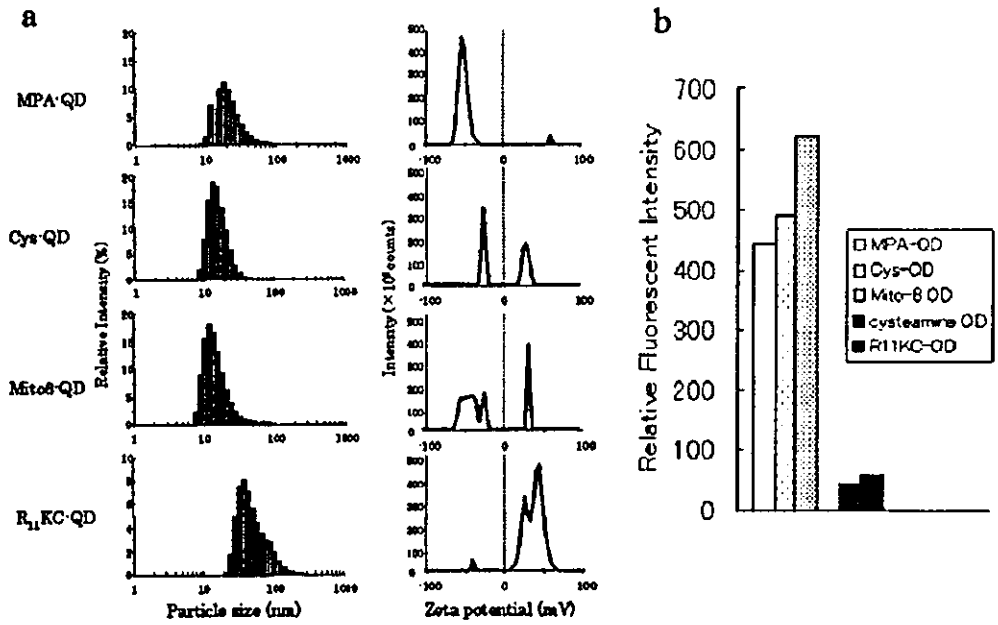

Fig. 2. Physicochemical properties of oligopeptide-conjugated QDs. (a) Particle size distribution of various QDs in aqueous solution (left) was measured by dynamic light scattering methods. Values are the mean±standard deviation of the data measured 12 times, respectively. Surface ζ-potential of QDs (right) was measured by electrophoresis. The line shows the electrophoretic mobility of these QDs in the stationary layers of 30 assays. Data shows the average of 30 assays. (b) Relative fluorescence intensity of QDs solution (10 μM) were measured by fluorospectrometer. QDs were excited by 365 nm wavelength (UV-A) and luminescence intensity of peak emission wavelength (519 nm) was detected.

acid at the first step, and secondarily coupled with the target oligopeptide. We prepare two kinds of QD whose surfaces were covered with carboxyl and sulfhydryl, and with NH_2 and hydroxyl groups, respectively. MPA-QDs were primarily coupled with amine groups of cysteine by using EDC coupling reagents (cys-QD). In the case of amine-QDs, they were also coupled with carboxylic groups of serine (ser-QD). The surface of the obtained QD was covered with approximately 450 amino acids per particle (data not shown). Both of the newly obtained amino acid-coated QDs, which were stable for changes of pH, were secondarily conjugated with target peptides by coupling with their sulfhydryl and amine groups by sulfo-SMCC reagents. In this study, we conjugated two kinds of signaling peptide; nuclear localizing signal (NLS) oligopeptide $R_{11}KC$ (25), and mitochondria targeting signal (MTS) oligopeptide Mito-8 (13). Mito-8 peptides were coupled with cys-QDs, and basic $R_{11}KC$-peptides were with ser-QDs, respectively. The number of peptide with QDs were calculated based on RC-DC protein assay, indicating that QD-$R_{11}KC$ and QD-Mito-8 were covered with 48 and 62 peptides per particle, respectively (data not shown). To assess the change of physicochemical properties of QDs after conjugated with oligopeptides, the particle size and surface potential of peptide-conjugated QDs were observed by a dynamic light scattering method. This surface potential of QDs was drastically changed after conjugated with peptides (Fig. 2a). In this labeling method, the average of the observed particle size distribution tends to increase, because it is hardly avoidable to control the excess polymerization. Previously, we tried to target signal peptides directly to MPA-QDs, resulted in aggregation, especially in the case of amine-rich oligopeptides because of salt-formation between carboxylic groups of QD and amine groups of target peptides (16). This novel two-step method enables to QDs labeled even in amine-rich basic oligopeptides such as $R_{11}KC$. Our previous study demonstrated that the fluorescence intensity of QD was also dramatically changed by the surface-covered molecules of QD particle (16, 22). We previously tried to cover QDs directly with cysteine monomer, which resulted in losing luminescence during the labeling process, because of electron leakage through the surface NH_2 group (16). Therefore, we assessed whether the fluorescent intensity of QDs changed or diminished during the peptide coupling process. After the first reaction step, slight change of luminescent intensity was observed. But the fluores-

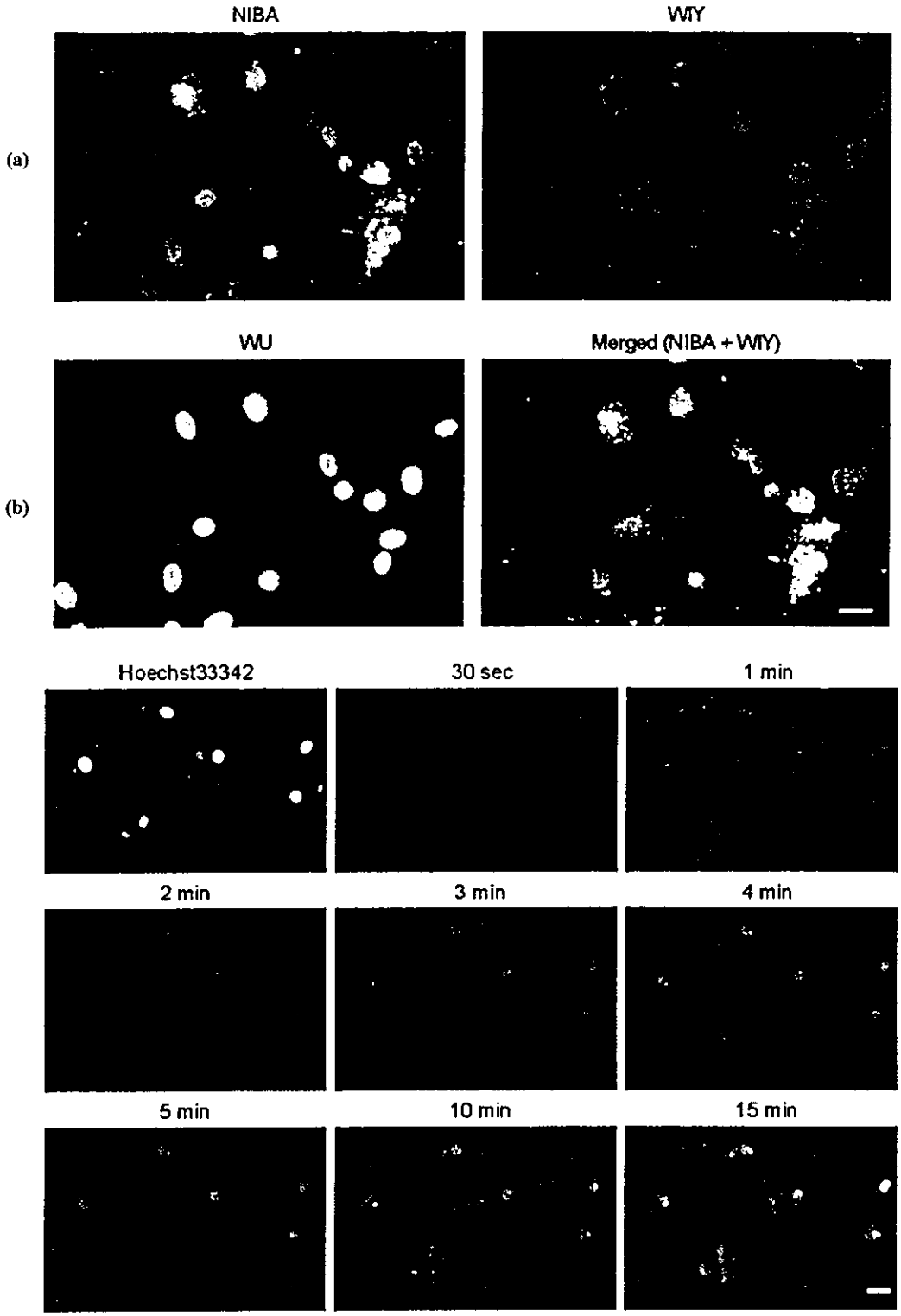

Fig. 3. Localization of R_{11}KC-conjugated QDs to nucleus. (a) Cells were pre-stained with Hoechst®33342, and stimulated with FITC-labeled QD-conjugated R_{11}KC peptide (1 μM final) for 3 hr at 37 C with 5% CO_2 condition. (b) Cells were pre-stained with Hoechst®33342, and stimulated with QD-R"KC (1 μM final) for the indicated time at 37 C under 5% CO_2 condition with a culture fluorescence microscope (IM-310 system, Olympus). Images were taken using D1X digital camera (Nikon) equipped with IM-310 system at the indicated time by a 3 sec exposure. Bars indicated 10 μm.

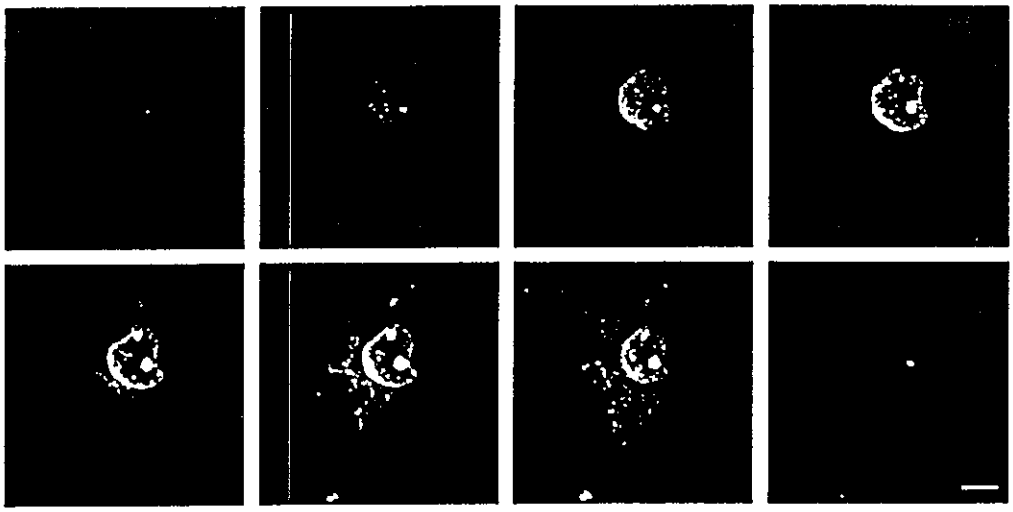

Fig. 4. R_{11}KC-conjugated QDs were accumulated in nucleous. Cells were stimulated by R_{11}KC-QD as described in Fig. 3. The cells were observed by confocal microscopy. The images are collected in the Z-direction at the span of 0.1 μm. Bars indicated 10 μm. Magnifications: ×120.

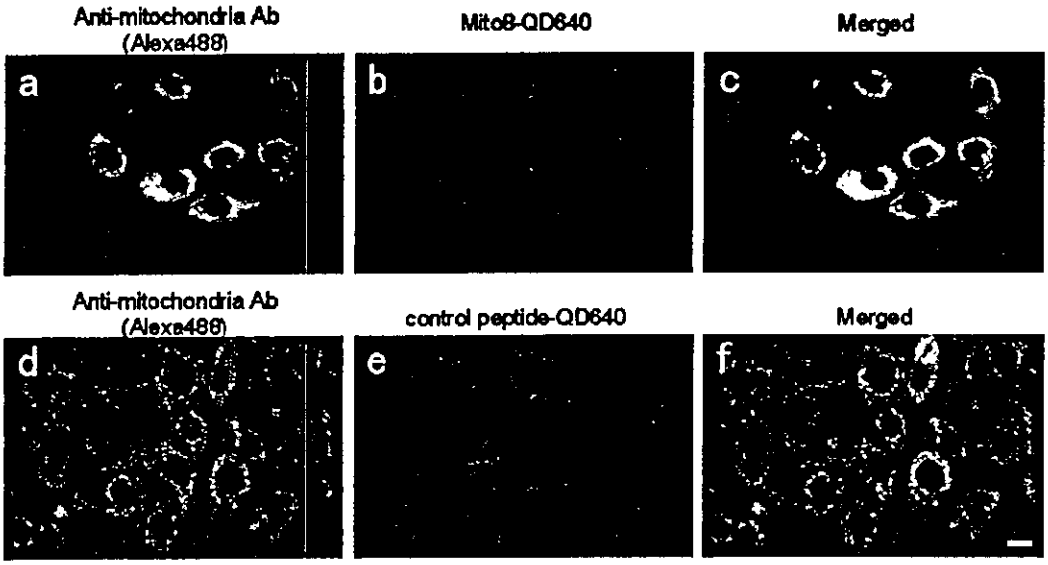

Fig. 5. Mitochondria images of Vero cells. Vero cells were stimulated with 1 μM with Mito-8 QD640 (a–c) or control START QD640 (d–f), and incubated for 12 hr under 37 C conditions. Cells were then fixed, and stained with anti-human mitochondria (M2) antibody. The cells were observed by fluorescent microscopy. Bars indicated 10 μm.

cence intensity enhanced remarkably after the secondary coupling with the target peptide (Fig. 2b). This result suggested that covering QD with the high molecular weight polymer such as polypeptides might prohibit the leakage of electron and might contribute to the continuative electron-rich condition of whole QD particle.

Next we evaluated whether the function of signal peptides would be held after conjugated with QDs. To confirm this, FITC-conjugated R_{11}KC peptides were conjugated with QD640 (fluorescence 640 nm, emitted red) and added to the cultured COS7 cells. We previously reported that QD without any peptides resulted in cellular-uptake into endosome by endocytotic pathways (17, 33). In this case, the red fluorescence from QD was located in nucleus and co-localized with that from FITC (Fig. 3a). This result indicated that QDs with nuclear peptides acquire another function that was based on R_{11}KC peptides. Unlabeled R_{11}KC remained in this study because the labeling efficiency of QDs with

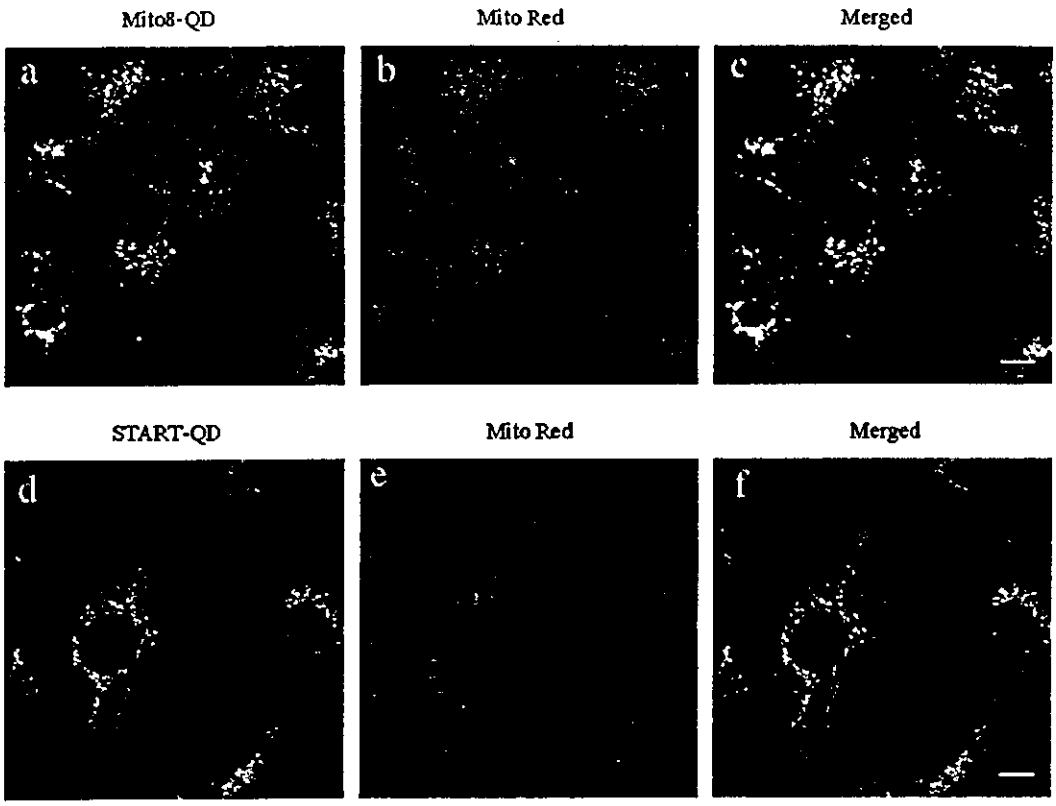

Fig. 6. Living mitochondria images by confocal microscope. Vero cells were cultured with 1 μM QD520-Mito8 (a–c) or QD520-START (control peptide, d–f) for 12 hr under 37 C conditions. Then cells were co-stimulated with MitoRed® mitochondria staining reagents (Dojindo Laboratories) for more additional 1 hr. After stimulation, cells were observed by confocal microscopy as shown in Fig. 4. Bars indicated 20 μm. Magnifications: ×80.

Fig. 7. Two kinds of signal peptide-QD showed independent behavior in the cells. Vero cells were co-stimulated with 1 μM QD640-Mito8 (emitted red) and QD-R_{11}KC (emitted green) for 12 hr under 37 C conditions. After fixed, the cells were observed by confocal microscopy. Bars indicated 20 μm.

oligopeptides was approximately 40% in this method and almost all of the FITC-tagged R_{11}KCs were not labeled with QDs. This result indicated that the R_{11}KC-QD has the same capability to localize into a nucleus as original ones. It is already reported that R_{11}KC peptide is rapidly localized into a nucleus by incubating for 10 min (25, 39). Then we tried to track the footmark of R_{11}KC peptide into nucleus in living cells for 15 min. Vero cells were treated with R_{11}KC-conjugated QD640 and continuously observed under a culture fluorescent microscopy (Fig. 3b). The penetration from the cell membrane to nuclei was observed about 30 sec after incubation, and precedently located into nucleus after 1 min. R_{11}KC-QDs were gradually accumulated the

whole nucleus during 15 min incubation. To investigate the localization of R_{11}KC-QDs into the nucleus, QDs distribution in the nucleus was observed by confocal microscopy (Fig. 4). R_{11}KC-QDs were dispersed in the whole nucleus and partially accumulated in nucleolus. In this study, we demonstrated that QDs as well as other fusion protein could also transit into nucleus with the help of nuclear signaling peptides.

Next we assessed the function of mitochondria signal peptides with QDs (Fig. 5). Mito-8 peptide- and control START peptide-coated QD640 (fluorescence 640 nm, emitted red) were incubated with cells and stained with anti-mitochondrial antibody. QD-red signal with Mito-8 gave raise to yellow in merged images (Fig. 5c). In contrast, red fluorescence emitted from control START peptides was not co-localized with that of mitochondria signal (Fig. 5f). Then we tried to visualize mitochondria distribution in living cells. Mito8-QD520 peptide was co-cultured with MitoRed® mitochondria staining dyes (Dojindo Laboratories, Japan). After incubation, the cells were observed by confocal laser microscopy (Fig. 6). QD-Mito-8 green luminescences from QD520 were also co-localized with conventional mitochondria probes. These results indicated that QDs with functional oligopeptides possessed dual functions to localize specific organelle and to emit high detectable fluorescence. Then we demonstrate the mixture of those two peptide separately move to their assigned organelle. The mixture of R_{11}KC-QD640 and Mito-8-QD520 were added to the Vero cells (Fig. 7). Red luminescence from R_{11}KC was separated from green ones from Mito-8 and not co-localized with each other, implying that QDs with functional peptides were individually transported to the target organelle.

Now several groups have reported that QDs conjugated with antibodies and some peptides for biological assays and cellular imaging *in vitro* and *in vivo* were demonstrated as brighter and longer lifetime probes (27–30). In this article, we demonstrated the various signal peptides conjugated with fluorescent QDs to both deliver QDs into living cells and selectively target specific organelles in living cells. In addition, these peptides-QD complexes have ability to translocate itself across the cell plasma membrane and can subsequently home to their specific targets such as the nucleus or the mitochondria. These results indicated that we succeeded in adding the new function as "information" to QDs by conjugating them with peptides. Our previous studies showed that QD-conjugated albumin and QD-glycerol can be targeted to the endosome and cytoplasm, respectively (14, 17). We showed in this article that QDs with targeted peptides can be also transported to nuclei and mitochondria. These techniques have the possibility that QDs can reveal transduction of proteins and peptides to specific subcellular compartments *in vitro* and even *in vivo* as a powerful tool for conducting intracellular analysis. We suggest that this technology could have a significant impact on the field of molecular and cellular biology as well as biotechnology. Recently, the plan that applied a novel nanomaterial such as nanocrystal QDs to the medical field attracted attention as one of the industrial applications of nanotechnology. And what is more, it is expected that QDs will be applied in the medical field for the innovative investigation, diagnosis and treatment of various diseases (8, 36, 38). It is very important to produce nanometer-sized materials with biological function, since we have no "designed material" which can arbitrarily penetrate nanometer-size gaps such as the skin, membrane, a blood vessel, and so on. This study demonstrates that these surface modifications of functional molecules combined with nanoparticles may work as bio-nanomachines conforming to the functions designated by their surface molecules. Nanomaterials have a great capacity of changing even the concept of existing diagnosis and medical treatment, by giving functions such as the pharmacological and magnetic effects, by giving the information of the specificity to tissue or organs *in vivo*. Novel nanomaterials including QD-supermolecules can be utilized as a transporter of the intracellular drug and gene delivery tools in the future.

We thank Mr. Kazuyuki Ito for valuable advice and help with proofreading. This work was supported by Medical Techniques Promotion Research Grant from the Ministry of Health, Labour and Welfare of Japan (H14-nano-004, Kenji Yamamoto).

References

1) Aglipay, J.A., Lee, S.W., Okada, S., Fujiuchi, N., Ohtsuka, T., Kwak, J.C., Wang, Y., Johnstone, R.W., Deng, C., Qin, J., and Ouchi, T. 2003. Oncogene **22**: 8931–8938.
2) Akerman, M.E., Chan, W.C., Laakkonen, P., Bhatia, S.N., and Ruoslahti, E. 2002. Nanocrystal targeting *in vivo*. Proc. Natl. Acad. Sci. U.S.A. **99**: 12617–12621.
3) Ballou, B., Lagerholm, B.C., Ernst, L.A., Bruchez, M.P., and Waggoner, A.S. 2004. Noninvasive imaging of quantum dots in mice. Bioconjugate Chem. **15**: 79–86.
4) Bruchez, M., Jr., Moronne, M., Gin, P., Weiss, S., and Alivisatos, A.P. 1998. Semiconductor nanocrystals as fluorescent biological labels. Science **281**: 2013–2016.
5) Chan, W.C., and Nie, S. 1998. Quantum dot bioconjugates for ultrasensitive nonisotopic detection. Science **281**: 2016–2018.
6) Dabboussi, B.O., Rodriguez-Viejo, J., Mikulec, F.V., Hein, J.R., Mattoussi, H., Ober, R., Jensen, K.F., and Bawendi, M.G. 1997. (CdSe)ZnS core-shell quantum dots; synthesis and characterization of size series of highly luminescent nanocrystallites. J. Phys. Chem. **101**: 9463–9475.

7) Dubertret, B., Skourides, P., Norris, D.J., Noireaux, V., Brivanlou, A.H., and Libchaber, A. 2002. *In vivo* imaging of quantum dots encapsulated in phospholipid micelles. Science **298**: 1759–1762.
8) Gao, X., Chan, W.C., and Nie, S. 2002. Quantum-dot nanocrystals for ultrasensitive biological labeling and multicolor optical encoding. J. Biomed. Opt. **7**: 532–537.
9) Gao, X., Cui, Y., Levenson, R.M., Chung, L.W.K., and Nie, S. 2004. *In vivo* cancer targeting and imaging with semiconductor quantum dots. Nat. Biotechnol. **22**: 969–976.
10) Gerion, D., Pinaud, F., Williams, S.C., Parak, W.J., Zanchet, D., Weiss, S., and Alivisatos, A.P. 2001. Synthesis and properties of biocompatible water-soluble silica-coated CdSe/ZnS semiconductor quantum dots. J. Phys. Chem. **105**: 8861–8871.
11) Goldman, E.R., Anderson, G.P., Tran, P.T., Mattoussi, H., Charles, P.T., and Mauro, J.M. 2002. Conjugation of luminescent quantum dots with antibodies using an engineered adaptor protein to provide new reagents for fluoroimmunoassays. Anal. Chem. **74**: 841–847.
12) Gorlich, D., and Mattaj, I.W. 1996. Nucleocytoplasmic transport. Science **271**: 1513–1518.
13) Haggie, P.M., and Verkman, A.S. 2002. Diffusion of tricarboxylic acid cycle enzymes in the mitochondrial matrix *in vivo*. Evidence for restricted mobility of a multienzyme complex. J. Biol. Chem. **277**: 40782–40788.
14) Hanaki, K., Momo, A., Oku, T., Komoto, A., Maenosono, S., Yamaguchi, Y., and Yamamoto, K. 2003. Semiconductor quantum dot/albumin complex is a long-life and highly photostable endosome marker. Biochem. Biophys. Res. Commun. **302**: 496–501.
15) Hines, M.A., and Guyot-Sionnest, P. 1996. Synthesis and characterization of strongly luminescing ZnS-capped CdSe nanocrystals. J. Phys. Chem. **100**: 468–471.
16) Hoshino, A., Fujioka, K., Oku, T., Suga, M., Sasaki, Y.F., Ohta, T., Yasuhara, M., Suzuki, K., and Yamamoto, K. 2004. Physicochemical properties and cellular toxicity of nanocrystal quantum dots depend on their surface modification. Nano Lett. **4**: 2163–2169.
17) Hoshino, A., Hanaki, K., Suzuki, K., and Yamamoto, K. 2004. The applications T-lymphoma labeled with fluorescent quantum dots to cell trafficking markers in a mouse body. Biochem. Biophys. Res. Commun. **314**: 46–53.
18) Ishii, D., Kinbara, K., Ishida, Y., Ishii, N., Okochi, M., Yohda, M., and Aida, T. 2003. Chaperonin-mediated stabilization and ATP-triggered release of semiconductor nanoparticles. Nature **423**: 628–632.
19) Jaiswal, J.K., Mattoussi, H., Mauro, J.M., and Simon, S.M. 2003. Long-term multiple color imaging of live cells using quantum dot bioconjugates. Nat. Biotechnol. **21**: 47–51.
20) Johnson, L.V., Walsh, M.L., and Chen, L.B. 1980. Localization of mitochondria in living cells with rhodamine 123. Proc. Natl. Acad. Sci. U.S.A. **77**: 990–994.
21) Kaether, C., and Gerdes, H.H. 1995. Visualization of protein transport along the secretory pathway using green fluorescent protein. FEBS Lett. **369**: 267–271.
22) Kaul, Z., Yaguchi, T., Kaul, S.C., Hirano, T., Wadhwa, R., and Taira, K. 2003. Mortalin imaging in normal and cancer cells with quantum dot immuno-conjugates. Cell Res. **13**: 503–507.
23) Larson, D.R., Zipfel, W.R., Williams, R.M., Clark, S.W., Bruchez, M.P., Wise, F.W., and Webb, W.W. 2003. Water-soluble quantum dots for multiphoton fluorescence imaging *in vivo*. Science **300**: 1434–1436.
24) Lidke, D.S., Nagy, P., Heintzmann, R., Arndt-Jovin, D.J., Post, J.N., Grecco, H.E., Jares-Erijman, E.A., and Jovin, T.M. 2004. Quantum dot ligands provide new insights into erbB/HER receptor-mediated signal transduction. Nat. Biotechnol. **22**: 198–203.
25) Matsushita, M., Tomizawa, K., Moriwaki, A., Li, S.T., Terada, H., and Matsui, H.J. 2001. A high-efficiency protein transduction system demonstrating the role of PKA in long-lasting long-term potentiation. J. Neurosci. **21**: 6000–6007.
26) Mattaj, I.W., and Englmeier, L. 1998. Nucleocytoplasmic transport: the soluble phase. Annu. Rev. Biochem. **67**: 265–306.
27) Mattoussi, H., Mauro, J.M., Goldman, E.R., Anderson, G.P., Sundar, V.C., Mikulec, F.V., and Bawendi, M.G. 2000. Self-assembly of CdSe-ZnS quantum dot bioconjugates using an engineered recombinant protein. J. Am. Chem. Soc. **122**: 12142–12150.
28) Medintz, I.L., Clapp, A.R., Mattoussi, H., Goldman, E.R., Fisher, B., and Mauro, J.M. 2003. Self-assembled nanoscale biosensors based on quantum dot FRET donors. Nat. Mater. **2**: 630–639.
29) Osaki, F., Kanamori, T., and Sando, S., Sera, T., and Aoyama, Y. 2004. Quantum dot conjugated sugar ball and its cellular uptake. On the size effects of endocytosis in the subviral region. J. Am. Chem. Soc. **126**: 6520–6521.
30) Pinaud, F., King, D., Moore, H.P., and Weiss, S. 2004. Bioactivation and cell targeting of semiconductor CdSe/ZnS nanocrystals with phytochelatin-related peptides. J. Am. Chem. Soc. **126**: 6115–6123.
31) Rizzuto, R., Brini, M., Pizzo, P., Murgia, M., and Pozzan, T. 1995. Chimeric green fluorescent protein as a tool for visualizing subcellular organelles in living cells. Curr. Biol. **5**: 635–642.
32) Rosenthal, S.J., Tomlinson, I., Adkins, E.M., Schroeter, S., Adams, S., Swafford, L., McBride, J., Wang, Y., DeFelice, L.J., and Blakely, R.D. 2002. Targeting cell surface receptors with ligand-conjugated nanocrystals. J. Am. Chem. Soc. **124**: 4586–4594.
33) Shibahara, A., Hoshino, A., Hanaki, K., Suzuki, K., and Yamamoto, K. 2004. On the cyto-toxicity caused by quantum dots. Microbiol. Immunol. **48**: 669–675.
34) Shubeita, G.T., Sekatskii, S.K., Dietler, G., Potapova, I., Mews, A., and Basch, T. 2003. Scanning near-field optical microscopy using semiconductor nanocrystals as a local fluorescence and fluorescence resonance energy transfer source. J. Microsc. **210**: 274–278.
35) Smith, A.M., Gao, X., and Nie, S. 2004. Quantum-dot nanocrystals for *in-vivo* molecular and cellular imaging. Photochem. Photobiol. (in press).
36) Su, X.L., and Li, Y. 2004. Quantum dot biolabeling coupled with immunomagnetic separation for detection of *Escherichia coli* O157:H7. Anal. Chem. **76**: 4806–4810.
37) Taguchi, T., Shimura, M., Osawa, Y., Suzuki, Y., Mizoguchi, I., Niino, K., Takaku, F., and Ishizaka, Y. 2004.

Nuclear trafficking of macromolecules by an oligopeptide derived from Vpr of human immunodeficiency virus type-1. Biochem. Biophys. Res. Commun. **320**: 18–26.

38) Voura, E.B., Jaiswal, J.K., Mattoussi, H., and Simon, S.M. 2004. Tracking metastatic tumor cell extravasation with quantum dot nanocrystals and fluorescence emission-scanning microscopy. Nat. Med. **10**: 993–998.

39) Wu, H.Y., Tomizawa, K., Matsushita, M., Lu, Y.F., Li, S.T., and Matsui, H. 2003. Poly-arginine-fused calpastatin peptide, a living cell membrane-permeable and specific inhibitor for calpain. Neurosci. Res. **47**: 131–135.

40) Wu, X., Liu, H., Liu, J., Haley, K.N., Treadway, J.A., Larson, J.P., Ge, N., Peale, F., and Bruchez, M.P. 2003. Immunofluorescent labeling of cancer marker Her2 and other cellular targets with semiconductor quantum dots. Nat. Biotechnol. **21**: 41–46.

41) Xu, H., Sha, M.Y., Wong, E.Y., Uphoff, J., Xu, Y., Treadway, J.A., Truong, A., O'Brien, E., Asquith, S., Stubbins, M., Spurr, N.K., Lai, E.H., and Mahoney, W. 2003. Multiplexed SNP genotyping using the Qbead system: a quantum dot-encoded microsphere-based assay. Nucleic Acids Res. **31**: 43.

NANO LETTERS

2004
Vol. 4, No. 11
2163−2169

Physicochemical Properties and Cellular Toxicity of Nanocrystal Quantum Dots Depend on Their Surface Modification

Akiyoshi Hoshino,[†,‡,§] Kouki Fujioka,[†] Taisuke Oku,[†] Masakazu Suga,[†] Yu F. Sasaki,[∥] Toshihiro Ohta,[⊥] Masato Yasuhara,[‡] Kazuo Suzuki,[§] and Kenji Yamamoto*[,†,‡]

Department of Medical Ecology and Informatics, Research Institute, International Medical Center of Japan, Toyama 1-21-1, Shinjuku, Tokyo 162-8655, Japan, Department of Pharmacokinetics and Pharmacodynamics, Hospital Pharmacy, Tokyo Medical and Dental University Graduate School, Yushima 1-5-45, Bunkyo-ku, Tokyo 113-8519, Japan, Department of Bioactive Molecules, National Institute of Infectious Diseases, Toyama 1-23-1, Shinjuku, Tokyo 162-8640, Japan, Faculty of Chemical and Biological Engineering, Hachinohe National College of Technology, Tamonoki Uwanotai 16-1, Hachinohe, Aomori 039-1192, Japan, and School of Life Science, Tokyo University of Pharmacy and Life Science, Horinouchi 1432-1, Hachioji, Tokyo 192-0392, Japan

Received August 9, 2004; Revised Manuscript Received October 5, 2004

ABSTRACT

Nanocrystal quantum dots (QDs) have been applied to molecular biology because of their greater and longer fluorescence. Here we report the potential cytotoxicity of our characterized QDs modified with various molecules. Surface modification of QDs changed their physicochemical properties. In addition, the cytotoxicity of QDs was dependent on their surface molecules. These results suggested that the properties of QDs are not related to those of QD-core materials but to molecules covering the surface of QDs.

The behavior of QDs in biological systems is not dependent on the chemical properties of surface-covered molecules but on the nanocrystal particle itself. The surface treatment of nanocrystals (surface-covered functional groups and biomolecules covering the surface of QDs) has specified the biological behavior of whole nanocrystal QDs.

With the development of nanotechnology engineering, nanomaterial products such as carbon nanotubes, fullerenes, and nanocrystal quantum dots (QDs) are now widely produced and consumed. Great quantities of those "artificial nanomaterials" have been used on the premise of being biologically and environmentally harmless, although only a few studies have reported the cellular toxicity of those materials.[1] These artificial nanomaterials are so small that they may be easily spread, stored in the environment and even in our body, and disrupt some functions of living organism consisting of complicated natural nanomaterials. It cannot be denied that these artificial nanomaterials are also detrimental, once small substances such as asbestos, coarse particulates, and particle matter exhaust from diesel engines proved to be harmful.[2−4] Thus, we need to investigate the potential toxicity of artificial nanomaterials.

QDs are now becoming widely used in biotechnology and medical applications.[5−12] QDs have several advantages over organic fluorophores with regard to high luminescence, stability against photobleaching, and a range of fluorescence wavelengths from blue to infrared depending on the particle size.[13] However, QDs aggregate easily and lose luminescence in an intracellular environment, even under acidic (pH < 5) or isotonic conditions. Therefore, it was considered difficult to replace conventional organic fluorescent probes completely with QDs.[14] Recently, some improvements were reported to prevent aggregation under intracellular conditions by the conjugation of biomolecules with QDs,[15−18] and some are used in immunohistochemical staining.[17−19] In this study, we developed several novel surface-modified QDs using carboxylic acids, polyalcohols, and amines and evaluated their physicochemical character and cytotoxicity. There are few

* Corresponding author. E-mail: backen@ri.imcj.go.jp. Tel: +81-3-3202-7181 ext 2856. Fax: +81-3-3202-7364.
† International Medical Center of Japan.
‡ Tokyo Medical and Dental University Graduate School.
§ National Institute of Infectious Diseases.
∥ Hachinohe National College of Technology.
⊥ Tokyo University of Pharmacy and Life Science.

10.1021/nl048715d CCC: $27.50
Published on Web 10/16/2004

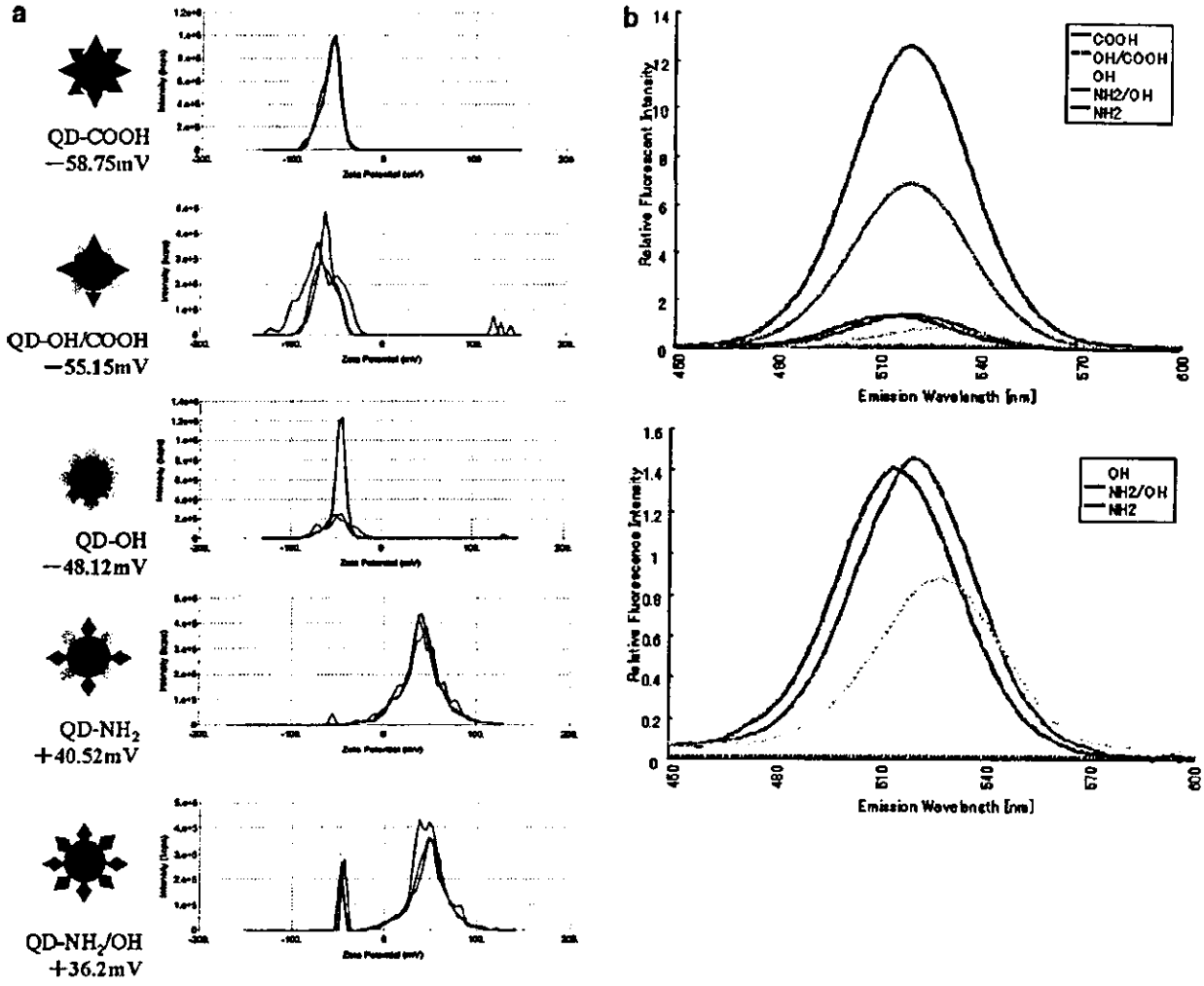

Figure 1. Surface ζ potential and fluorescence intensity of QDs varied by their surface modification. (a) Cartoon (left) and ζ potential (right) of the novel modified QDs. Surface zeta-potential of QDs is measured by electrophoresis. Each line shows the electrophoretic mobility of QDs in the stationaly layers. The data are the average of 30 assays. (b) Relative fluorescence intensity and peak wavelength of QDs measured by fluorescence spectrometry. (Lower) enlarged panel of QD-OH (yellow); QD-NH_2/OH (green) and QD-NH_2 (blue) in the upper panel. The peak emission wavelengths of QD-COOH, QD-OH/COOH, QD-OH, QD-NH_2/OH, and QD-NH_2 varied at 519, 520, 526, 520, and 513 nm, respectively.

studies on the cytotoxicity of QDs in mammalian cells, although several experiments applying to living cells and animals have already been performed.[19−25] In this study, we tested the cytotoxic potential of QDs by three different assays: comet assay, flow cytometry, and MTT assay. The comet assay, which detects DNA damage by gel electrophoresis, has been widely used to detect apoptotic cell damage induced by chemicals.[26−29] In this assay, DNA fragments can be observed as a stream from the nucleus, and the level of damage can be quantitated by the length of the stream of DNA fragments. We report here that the cytotoxicity of QDs is also caused by the surface-covering molecules of QDs but not by the nanocrystalline particle itself.

We synthesized ZnS-coated CdSe nanocrystal QDs (518-nm fluorescence peak emission). Synthesized QDs were then coated with MUA (QD-COOH), cysteamine (QD-NH_2), or thioglycerol (QD-OH) using thiol-exchange reactions as previously described.[30−32] To introduce two functional groups (QD-OH/COOH, and QD-NH_2/OH), we used equal molar quantities of thioglycerol and MUA or cysteamine and thioglycerol, respectively. To investigate the physicochemical properties of these five types of modified QDs, we measured the fluorescence intensity, particle diameter, and surface ζ potential. At first, we assessed the surface ζ potential of QDs to confirm whether the exchange reaction was performed (Figure 1a). As expected, QD-COOH and QD-OH/COOH were highly negatively charged, whereas QD-NH_2 and QD-NH_2/OH were positively charged. QD-OH was less negatively charged than the carboxylic acid groups. QDs with both hydroxyl and carboxyl/amine groups had median charge in both groups. We then assessed whether the difference in the surface modification of QDs affected the fluorescence intensity. The fluorescence intensity and peak wavelength

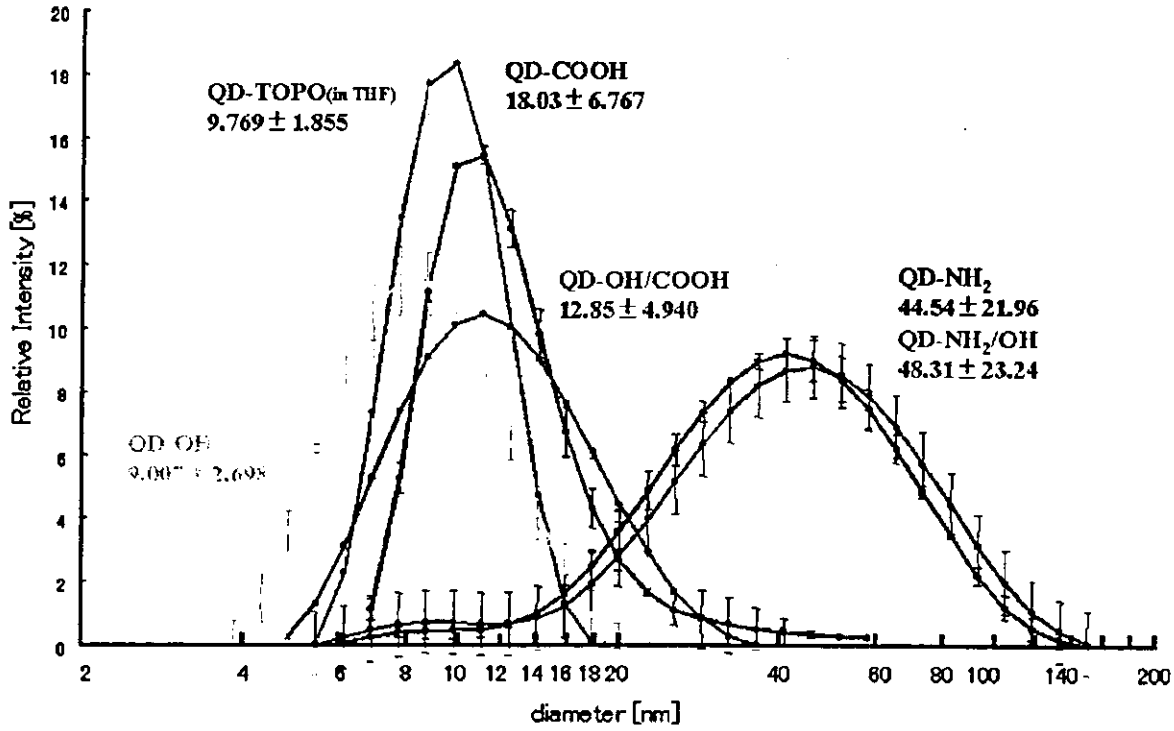

Figure 2. Size distribution of modified QDs in aqueous solution varied by their surface modification. The profile for the distribution of QDs in aqueous solution was observed by dynamic light scattering methods. Values are the mean ± standard deviation of the data measured 12 times, respectively.

were measured using a fluorescence spectrometer (Figure 1b). The QDs of carboxyl groups had higher luminescence than the other groups. Furthermore, the peak wavelength varied according to the surface modification. QDs containing amino groups emitted a shorter wavelength than the originally synthesized QD (TOPO capped-QD; 518-nm emission). In contrast, QDs with hydroxyl groups were slightly red-shifted. We assumed that a longer carbon chain and the carboxyl groups of MUA may contribute to the long lifetime and high quantum yield of QD-COOH. In contrast, the decreasing fluorescence of amino-QD particles may be caused by the oxidation of QD-metal because of the leakage of electrons from QDs through NH_2 groups in aqueous solution.[13] This suggested that the luminescence intensity of QDs may increase according to the surface-covered molecule structures.

Although it is known that the fluorescence of QDs depends on the particle size, the interparticle conformation of QDs in aqueous solution has not yet been revealed. To investigate whether any change in the particle conformation of QDs occurred in the process of surface modification, we attempted to measure the particle diameter of QDs by dynamic light scattering (DLS). We used a He−Ne laser (633-nm wavelength) light source because using a short wavelength that excites the QDs impedes the detection of QD light scattering. The size distribution of QDs was widely spread according to their modifications (Figure 2). Amino-QDs showed a broad particle distribution around 40 nm. In contrast, QDs of carboxyl groups had a narrow distribution around 20 nm. These results seemed to be contradicted by the observation that the emission wavelength of QDs depended on their particle size.[11,34] In addition, it was previously reported that transmission electron microscopy showed the diameter of the uncoated green nanocrystalline QD to be approximately 3.5 nm.[31] Positively charged amino-QDs and negatively charged impure materials in solution (such as TOPO) may form an ionic combination and affect the "apparent" diameter of the particles. In the case of carboxyl QDs, hydrophobic interaction among long carbon chains is also concerned with their larger particle distribution.

Processing the QD surface with hydroxyl group resulted in improved dispersion and stability under hypertonic conditions (Figure 3). In contrast, all of the QDs were stable in nonelectrolyte solutions. All of the modified QDs were stable for 30 min under weak alkaline conditions, whereas only QDs of the amine groups were stable under acidic conditions. These results were useful for advanced surface development to apply QDs in biological and medical fields.

To examine whether QDs affected cell proliferation, we first assessed cell proliferation by MTT assay. The reduction activity of cells was decreased by adding the crude QDs (Figure 4), but we cannot determine whether the amine-QDs were harmful because MTT reagensts were nonbiologically reduced to hormazan by the amine-QDs (data not shown). Then we determined whether this damage was caused by cell death or the suppression of cell activity. To examine whether the cell damage of QDs was affected by their surface potential, the cytotoxicity was evaluated by flow